A tunable hybrid electro-magnetomotive NEMS device for low temperature physics

Eddy Collin, Thomas Moutonet, Jean-Savin Heron, Olivier Bourgeois, Yu. M. Bunkov, Henri Godfrin

Journal of Low Temperature Physics manuscript No.
(will be inserted by the editor)

E. Collin[1] · **T. Moutonet**[1] · **J.-S. Heron**[1] · **O. Bourgeois**[1] · **Yu.M. Bunkov**[1] · **H. Godfrin**[1]

A tunable hybrid electro-magnetomotive NEMS device for low temperature physics

14.07.2010

Keywords mechanics, NEMS, low temperatures, non-linearity

Abstract Microfabrication techniques have made possible the realization of mechanical devices with dimensions in the micro- and nano-scale domain. At low temperatures, one can operate and study these devices in well-controlled conditions, namely low electrical noise and cryogenic vacuum, with the ability to use high magnetic fields and superconducting coating metals[1]. Moreover, the temperature turns out to be a control parameter in the experimental study of mechanical dissipation processes, with the cryogenic environment ensuring that only low energy states are thermally populated. Immersed in a quantum fluid, these MEMS and NEMS devices (micro and nano electro-mechanical systems) can probe the excitations of the liquid at a smaller scale, with higher frequencies and better resolution than "classical" techniques[2]. We present experimental results obtained in vacuum on cantilever NEMS structures which can be both magnetomotive and electrostatically driven. The device is extremely sensitive with resolved displacements down to 1 Å using conventional room-temperature electronics. It is calibrated *in-situ*, and frequency/non-linearity can be tuned electrostatically. The design should allow parametric amplification to be used.

PACS numbers: 62.20.Dc, 62.40.+i, 81.40.Jj, 47.45.-n, 47.45.Ab

1 Introduction

Since the first experiments using taught superconducting wires immersed in a (quantum) fluid[3], "vibrating wires" are nowadays a classic probe used by low temperature physicists. The technique, later adapted in the form of semi-circular filament loops, gives access to the viscosity of the fluid through the damping and

Institut Néel
CNRS et Université Joseph Fourier,
BP 166, 38042 Grenoble Cedex 9, France
E-mail: eddy.collin@grenoble.cnrs.fr

the frequency shift measured on the structure's mechanical back-and-forth resonance (fundamental out-of-plane flexural mode). The lowest temperatures ever achieved in superfluid ^{3}He have been measured by vibrating wires[4,5] directly *inside* the liquid. Extremely sensitive cosmic particle detectors have been realized with superfluid ^{3}He bolometers using vibrating wires[6]. The low temperature mechanics of these superconducting filaments (in vacuum) has been extensively studied, down to below a milliKelvin[7].

While many groups have been employing quartz tuning forks to replace vibrating wires[8,9,10], the Grenoble group has been working on "goal-post" shaped silicon devices[2]. Indeed, aluminum and niobium-coated MEMS[(1)] were tested in the range 1 K - 30 K, and they displayed perfectly suitable characteristics[1,11]: low dissipation, rather high frequencies and controlled non-linearities. The versatility of microfabrication enables to make complex designs, scaling down the sizes from MEMS to NEMS[(2)], the latter[12] displaying frequencies in the MHz range with quality factors of the order of $10^3 - 10^4$. Moreover, our cantilever-based geometry is perfectly well suited for low temperature mechanics experiments, probing materials characteristics and non-linear dynamics. These issues are essential to the realization of optimal probes, and devices meant to be brought to their quantum limit[13,14].

In the present article we report on the realization, the first low temperature measurements together with our calibration method of an 8 MHz NEMS goal-post shaped device mimicking the vibrating wire geometry, having both an electromotive and magnetomotive drive. The system's resonance can be widely tuned with a DC voltage, the non-linearity can be adjusted, the magnetomotive drive and detection are perfectly linear while the non-linear electromotive scheme enables parametric drive/amplification to be used.

2 Experimental details

The NEMS device is obtained from thick SOI wafers (composed of a 150 nm silicon layer and a 1000 nm sacrificial silicon oxide layer)[15]. After an e-beam lithography, the structure is patterned by means of Reactive Ion Etching (with SF_6 through an Al mask). The 1000 nm oxide is then removed by a chemical vapor HF etching, releasing the vibrating element. As a last step, after stripping the initial Al mask a thin 50 nm layer of (unstrained) aluminum is deposited on the whole chip.

The device is composed of a mobile goal-post structure (two feet linked by a paddle), plus a capacitively coupled gate electrode separated by a 100 nm gap (total capacitance to ground measured to be 300 fF, see below). The gate electrode is directly connected to a voltage source, while the goal-post part is connected to a current source (1.1 kΩ resistor) and a lock-in amplifier (detection, 1 MΩ input). The NEMS mobile part metallic layer is about 110 ± 10 Ω at 4.2 K, in a 4-wire low frequency resistive measurement. The device is glued on a temperature-regulated copper plate sitting in a vacuum chamber ($P< 10^{-6}$ mbar). A DC magnetic field is

[1] MEMS: micro-electro-mechanical-systems.
[2] NEMS: nano-electro-mechanical-systems.

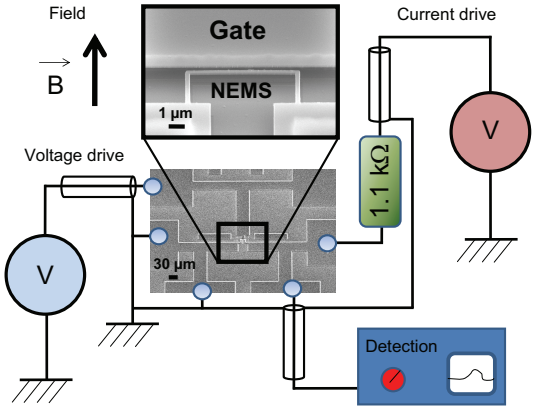

Fig. 1 (Color online) NEMS device. The structure is goal-post shaped, with 3 μm feet, 7 μm paddle, 250 nm width and 150 nm thickness. Also shown is a drawing of the detection and drives schemes (generators V, the left one corresponding to the gate voltage with a DC and an AC contribution, and the right one to the AC current drive). The cylinders represent coaxial cables (typ. few meters of low loss, 100 pF/m). A static magnetic field **B** created by a superconducting coil lies along the sample.

imposed along the sample. An SEM (Scanning Electron Microscope) picture with a drawing of the experimental setup is given in Fig. 1.

The magnetomotive excitation and detection scheme is adapted from the standard vibrating wire technique. A sinusoidal current $I_0\,cos(\omega t)$ is fed in the goal-post structure's metallic layer which lies in a static magnetic field B. A magnetomotive force $F_{mag} = I_0\,l\,B\,cos(\omega t)$ appears pulling the structure out of the plane (l is the length of the pad). As the angular frequency ω is swept through the mode resonance ω_0 the structure starts to vibrate and an induced voltage $V = l\,B\,dx(t)/dt$ appears at its ends (with x the top end displacement). It is detected with the lock-in amplifier, giving access to phase (X) and quadrature (Y) signals (electric homodyne detection).

The electromotive drive consists in a voltage $V_{dc} + V_0\,cos(\omega' t + \varphi)$ applied on the capacitively coupled electrode. A phase φ can be imposed between the current drive and the voltage drive. The driving force obtained (on the mobile part) is thus:

$$F_{elec} = +\frac{1}{2}\frac{\partial C(x)}{\partial x}\left(V_{dc}^2 + \frac{V_0^2}{2} + 2V_{dc}V_0\cos(\omega' t + \varphi) + \frac{V_0^2}{2}\cos(2\omega' t + 2\varphi)\right) \quad (1)$$

with $C(x)$ the capacitance of the gate to the goal-post NEMS. Writing a series expansion of the capacitance brings:

$$\frac{\partial C(x)}{\partial x} = \frac{\partial C(x=0)}{\partial x} + \frac{\partial^2 C(x=0)}{\partial x^2}x + \frac{1}{2}\frac{\partial^3 C(x=0)}{\partial x^3}x^2 + \frac{1}{6}\frac{\partial^4 C(x=0)}{\partial x^4}x^3. \quad (2)$$

We immediately realize from Eqs. (1) and (2) that the applied voltage will allow us to :

– drive the NEMS, i.e. first term in Eq. (2),

– tune the resonance frequency, i.e. second term in Eq. (2),
– and adjust the Duffing-like non-linear coefficient, last terms in Eq. (2).

Clearly, the resonance frequency tuning can be used for parametric amplification (and drive) with a proper choice of the voltage drive frequency ω' [16].
Note that neither the current drive, the voltage drive, nor the detection lines are 50 Ω adapted, in order to provide a high impedance isolating environment for the NEMS. At about 8 MHz (NEMS resonance frequency $f_0 = \omega_0/2\pi$) the true drives and detected amplitudes have to be carefully calibrated. We note $G_I(\omega)$ the losses on the current line, $G_V(\omega)$ on the voltage line and $G_D(\omega)$ on the detection (defined as the ratio of the voltage experienced at the NEMS device to the one measured at room temperature). Below 0.5 MHz, all the G_i are measured to be 1 to % accuracy.

3 Results

In Fig. 2 (bottom part) we show the characteristic displacement versus (magneto-motive) force curve at 4.2 K in vacuum. The graph has been obtained after having carefully calibrated G_I and G_D, with the procedure described below. In the insets, we show the resonance lines measured at the two extremes of the curve: very small and very large displacements. All these data are taken without any voltage applied to the gate.
Note the very large dynamic range spanned by our experiment, more than 3 orders of magnitude. We see both a non-linear damping characteristic of the aluminum coating, similar to the one observed in MEMS devices [11,1] (slight curvature at the top end of the x vs F_0 curve), and a non-linear Duffing-like contribution which distorts the resonance lines. This Duffing-like non-linear signature on our device is exceptionally small, for 0 V on the gate electrode (the right inset in Fig. 2 looks practically as Lorentzian as the left one). Indeed, a cantilever structure is inherently less non-linear than a doubly clamped beam. However, our non-linear contribution is *even smaller* than what we expected for a geometrical non-linear behavior [12]. We have tested different NEMS structures with similar aspect ratios and geometries, but different coating metals. For all these structures, we obtain *noticeably different* non-linear behaviors, while in the case of pure geometrical non-linearities in MEMS the signature is similar [17]. We thus have to attribute the small non-linear behavior to a (at least) partial cancellation of the geometrical non-linear behavior by materials non-linear contributions.
On the other hand, we can artificially increase the non-linearity with a gate voltage, generating hysteresis in the device (top graph, Fig. 2).

In Fig. 3 we present the resonance frequency tunability obtained through the voltage applied on the gate electrode. In Eq. (1), we first use V_{dc} to obtain the theoretical parabola and define the second coefficient of Eq. (2), i.e. $\partial^2 C/\partial x^2$. The tunability is of the order of 200 kHz per 10 V and positive, which is in agreement with the literature for out-of-plane motion [18] (NEMS-electrode gap of 400 nm), and larger by about a factor of 4 (our gap is 100 nm). Note that for our distorted structure [12], the tunability was much smaller and *negative*, consistent with Ref. [18] for a motion corresponding to an in-plane configuration.
Secondly, we use V_0 at various frequencies ω and scale the obtained parabola on

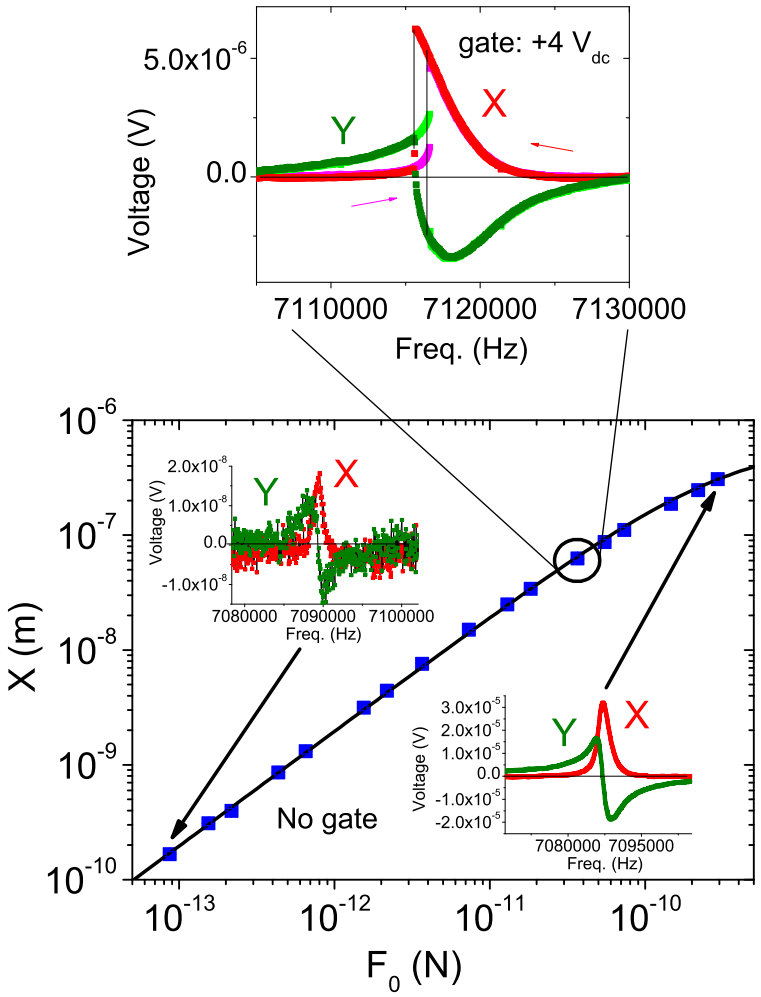

Fig. 2 (Color online) Displacement x versus magnetomotive force F_0 at 4.2 K in vacuum (values quoted in *rms*, no voltage on the gate). The field was typically smaller than a Tesla, with currents smaller than 50 μA. The left inset corresponds to the smallest excitations (displacement about 1.5 Å), while the right inset corresponds to the largest (about 300 nm). Red is the X component while green is the Y. The resonance line corresponding to the circled datapoint, measured with a gate +4 V DC bias is shown at the top, demonstrating voltage-induced hysteresis (dark and light colors, arrows) which is evidence for a non-linear behavior.

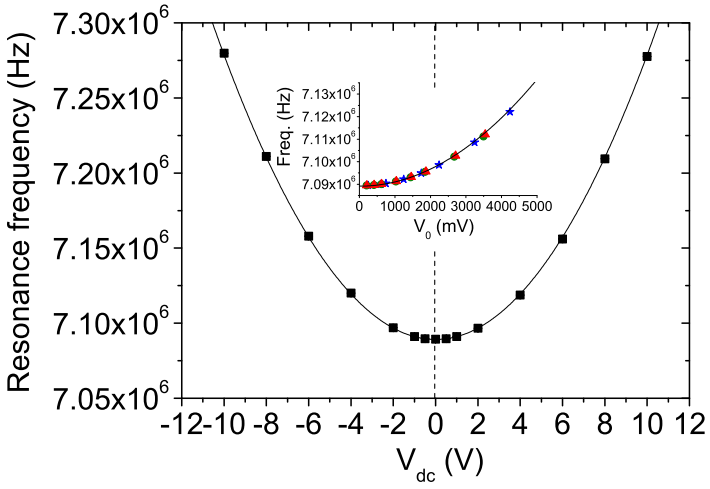

Fig. 3 (Color online) Tunability of the resonance, in the linear regime (small displacements), at 4.2 K in vacuum. The black squares are obtained by varying V_{dc} and keeping $V_0 = 0$. The green dots are $V_{dc} = 0$, $\omega/2\pi = 3.6$ MHz, the red triangles are $V_{dc} = 0$, $\omega/2\pi = 7.2$ MHz and the blue stars are $V_{dc} = 0$, $\omega/2\pi = 14.4$ MHz. The fit is the theoretical parabola, yielding the second coefficient of Eq. (2).

the DC result, yielding $G_V(\omega)$. We chose the frequencies to be off resonant with the NEMS, in order to safely neglect the oscillating terms in Eq. (1).
Knowing $G_V(\omega)$, we then apply a voltage on the gate electrode at various (non-resonant) frequencies, and measure the current obtained in the NEMS with the lock-in amplifier (i.e. on the metallic layer 110 Ω). We fit the result with a capacitance for the gate electrode of 300 fF (total value including parasitic couplings from the pads to ground strips), plus a low-pass filter composed of the 110 Ω in parallel with the detection coaxial cable, Fig. 4. We thus obtain $G_D(\omega)$.
Finally, we drive a current through the NEMS at various (non resonant) frequencies, and measure again on the NEMS' 110 Ω the obtained voltage. Knowing $G_D(\omega)$, we can determine $G_I(\omega)$ which is also fitted to a low-pass filter, Fig. 4. The modeling is very good up to 8 MHz; the calibration procedure is pursued at higher frequencies, but the results cannot be fitted by simple low-pass expressions due to complex reflexion patterns occurring in the impedance mis-matched lines.
The present procedure is very accurate, and relies only on the scaling of the AC measurements on the DC ones, knowing properly the drive resistor of the current source (for us, 1.1 kΩ). It enables to plot Fig. 2 in real units, thus weighting the NEMS structure. We obtain the effective values $m = 1.3\,10^{-15}$ kg for the mass and $k = 2.55$ N/m for the spring constant, consistent with calculations.

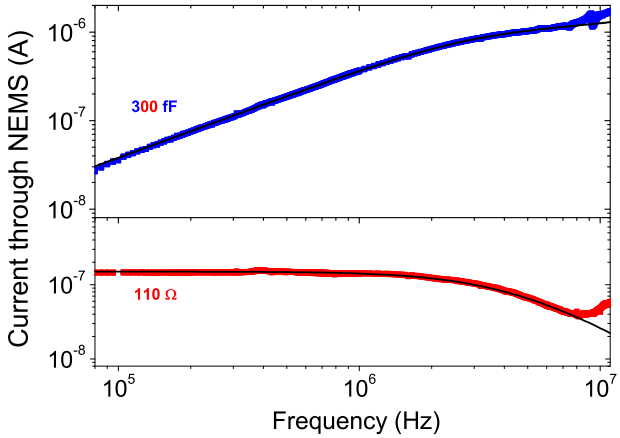

Fig. 4 (Color online) *In-situ* calibration of the lines (4.2 K). Top: defining the detection gain $G_D(\omega)$ by measuring the current through the NEMS when driving the capacitance with an AC drive $V_0 = 100$ mV$_{rms}$. Bottom: defining $G_I(\omega)$ while driving the NEMS with a current $I_0 = 160$ nA$_{rms}$. Black lines are low-pass fits explained in the text.

4 Conclusions

We present experimental results obtained on an 8 MHz NEMS at 4.2 K. The device has an extremely broad dynamic range down to very small displacements (1 Å), and can be both actuated with an electromotive and a magnetomotive force. The resonance frequency can be tuned with a DC voltage over a wide range. We demonstrate that the setup can be calibrated in situ to obtain true forces and displacements in m and N respectively. The capacitive coupling enables also to tune the Duffing-like non-linearity, or to use parametric amplification schemes.

Acknowledgements We wish to acknowledge the support of Thierry Fournier and Olivier Exshaw, and the support from MICROKELVIN, the EU FRP7 low temperature infrastructure grant 228464.

References

1. E. Collin, Laure Filleau, Thierry Fournier, Yuriy M. Bunkov and Henri Godfrin, *J. of Low Temp. Phys.* **150**, no 5-6, p. 739 (2008).
2. S. Triqueneaux, E. Collin, D. J. Cousins, T. Fournier, C. Bäuerle, Yu. M. Bunkov and H. Godfrin, *Physica B* **284**, p. 2141 (2000).
3. M.A. Black, H.E. Hall, K. Thomson, *Proc. 10th Int. Conf. on Low Temperature Physics*, p. 174 (1966); M.A. Black, H.E. Hall, K. Thomson, *J. Phys. C: Solid St. Phys.* **4**, p. 129 (1971).

4. A.M. Guénault, V. Keith, C.J. Kennedy, S.G. Mussett and G.R. Pickett, *J. of Low Temp. Phys.* **62**, p. 511 (1986).
5. C. Bäuerle, Yu.M. Bunkov, S.N. Fisher and H. Godfrin, *Phys. Rev. B* **57**, p. 14381 (1998); C.B. Winkelmann, E. Collin, Yu.M. Bunkov, H. Godfrin, *J. of Low Temp. Phys.* **135**, p. 3 (2004).
6. C.B. Winkelmann, J. Elbs, Yu.M. Bunkov, E. Collin, H. Godfrin, M. Krusius, *Nuclear Instr. and Methods in Physics Research* **A 574**, p. 264 (2007).
7. R. König, P. Esquinazi and F. Pobell, *J. of Low Temp. Phys.* **90**, p. 55 (1993).
8. D. O. Clubb, O. V. L. Buu, R. M. Bowley, R. Nyman et J. R. Owers-Bradley, *J. Low Temp. Phys.*, **136, Numbers 1-2**, (july 2004). DOI: 10.1023/B:JOLT.0000035368.63197.16
9. R. Blaauwgeers, M. Blazkova, M. Clovecko, V. B. Eltsov, R. de Graaf, J. Hosio, M. Krusius, D. Schmoranzer, W. Schoepe, L. Skrbek, P. Skyba, R. E. Solntsev et D. E. Zmeev, *J. Low Temp. Phys.*, *146, Numbers 5-6*, (march 2007). DOI: 10.1007/s10909-006-9279-4
10. M. Blazkova, M. Clovecko, V. B. Eltsov, E. Gao, R. de Graaf, J. J. Hosio, M. Krusius, D. Schmoranzer, W. Schoepe, L. Skrbek, P. Skyba, R. E. Solntsev et W. F. Vinen, *J. Low Temp. Phys.*, **150, Numbers 3-4**, (february 2008). DOI: 10.1007/s10909-007-9587-3
11. E. Collin, J. Kofler, S. Lakhloufi, S. Pairis, Yu. M. Bunkov, and H. Godfrin, *Journal of Applied Physics* **107, Issue 11**, 114905 (7 June 2010).
12. E. Collin, J. Kofler, J.-S. Heron, O. Bourgeois, Yu. M. Bunkov, H. Godfrin, *J. of Low Temp. Phys.* **158, Issue 3**, p. 678 (2010); the NEMS had a large distorsion due to stress which has to be taken into account (about 53° at the end tip) for a quantitative definiton of m and k. Correct parameters are $m = 32.10^{-15}$ kg and $k = 0.47$ N/m.
13. M. D. LaHaye, O. Buu, B. Camarota, K. C. Schwab, *Science* **304**, p. 74 (2004).
14. A. D. O'Connell, M. Hofheinz, M. Ansmann, Radoslaw C. Bialczak, M. Lenander, Erik Lucero, M. Neeley, D. Sank, H. Wang, M. Weides, J. Wenner, John M. Martinis, A. N. Cleland *Nature* **464**, 697-703 (17 March 2010).
15. J.-S. Heron, T. Fournier, N. Mingo and O. Bourgeois, *Nano Letters* **9**, 1861 (2009).
16. Barry E. DeMartini, Jeffrey F. Rhoads, Kimberly L. Turner, Steven W. Shaw, and Jeff Moehlis, *J. of MEMS* **16**, number 2, 310 (April 2007).
17. E. Collin *et al.*, submitted to *Phys. Rev. B* (2010).
18. I. Kozinsky, H. W. Ch. Postma, I. Bargatin, and M. L. Roukes, *Appl. Phys. Lett.* **88**, 253101 (2006).